D. Moulton, A. Fil, O. Myatra, B. Lipschultz, B. Dudson

Recent modelling of long-legged divertor configurations

Recent modelling of long-legged divertor configurations

D. Moulton, A. Fil, O. Myatra, B. Lipschultz, B. Dudson

RECENT SOLPS MODELLING OF LONG-LEGGED DIVERTOR CONFIGURATIONS

D. MOULTON, A. FIL, O. MYATRA, L XIANG
UKAEA-CCFE, Culham Science Centre
Abingdon, United Kingdom
Email: david.moulton@ukaea.uk

B. LIPSCHULTZ, B. DUDSON
Department of Physics, University of York
York, United Kingdom

Abstract

The paper reviews recent SOLPS modelling of long-legged divertors carried out by UKAEA and the University of York. The required upstream density required for detachment is predicted to scale inversely with the total flux expansion of the divertor, but experimentally this was not found to be the case on TCV. Interpretative SOLPS-ITER modelling suggests this to be a result of the confounding variable of neutral trapping; when neutral trapping is artificially equalised in the simulations, the effect of total flux expansion is as expected. Analysis of predictive MAST-U Super-X simulations suggests that the detachment front location in parallel space becomes less sensitive to control parameters (i.e. more easily controlled) in regions of high magnetic field strength gradient. The same simulations also suggest recombination sinks to be present only in deeply-detached simulations with relatively high upstream density and low impurity fraction (driven by deuterium fuelling). In equally-detached simulations with lower upstream density and higher impurity fraction (driven by impurity seeding), recombination was negligible. Deuterium ion-molecule elastic collisions are necessary for this qualitative difference. Finally, the relevance of long-legged divertors is investigated on DEMO. The engineeringly-feasible increase in outer divertor connection length is found to significantly increase the operational margin compared to the standard ITER-like DEMO divertor, approximately in line with simple Lengyel Model estimates.

1. INTRODUCTION

It is likely that fusion reactors will necessitate, or at least benefit from, 'advanced' divertor geometries. By improving the power handling of the divertor and the ease with which detachment can be controlled, advanced divertors are designed to expand the reactor's operational space, where core and exhaust requirements overlap. One way to achieve this is by increasing the divertor leg length to create a 'long-legged' divertor. The first attribute that all long-legged divertors share is increased parallel connection length from the target to the 'upstream' location, where power crosses from the core into the SOL. The second attribute often found in long-legged divertors is 'total flux expansion', $B_{upstream}/B_{tatrget} \approx R_{target}/R_{upstream}$; if this is significantly greater than unity then the configuration is termed 'Super-X' [1] and, as the total field strength decreases along the field line at larger major radius R, the parallel heat flux drops due to the increase in flux tube area. Finally, the third attribute, that is often enabled by the increased distance between core and divertor in long-legged geometries, is improved neutral confinement in the divertor through baffling.

Deciding whether long-legged divertors should be employed in future reactors requires quantification of the exhaust improvements they will provide, as well as the engineering cost against which those improvements must be balanced. Here, we review recent work towards this goal, carried out by UKAEA and the University of York, through interpretive and predictive SOLPS-ITER modelling of long-legged divertors on TCV, MAST-U and DEMO. This modelling addresses some of the key issues which will determine the efficacy of the long-legged divertor, including detachment onset, detachment sensitivity, and reactor relevance. It also includes more general analysis of the deeply-detached state that is likely to be relevant to conventional divertors as well. Each of the proceeding paper sections discusses one of these key issues. Results are given in more detail in the references provided.

2. DETACHMENT ONSET

Simple analytic models [2],[3] predict that the required upstream density for detachment $n_{upstream,onset}$ onset scales with (amongst other things) the inverse of total flux expansion in the divertor:

$$n_{upstream,onset} \propto B_{target}/B_{upstream} \approx R_{upstream}/R_{target} \, , \qquad (1)$$

where B is the total magnetic field strength and R is the major radius. There is some additional dependence on the parallel profile of B along the flux tube of interest, but this is weak compared to the dependence on the values of B at either end of that flux tube.

In [4], the dependence given by (1) was confirmed in SOLPS-5.0 simulations, using a novel "box divertor" geometry, which allowed $B_{upstream}/B_{target}$ to be varied independently of all other input variables (something that would be impossible to achieve in a realistic geometry). In a straight-down box with $B_{upstream}/B_{target}=1$, the rollover in target density (and target ion flux) was observed to occur at almost exactly twice the upstream density compared to a straight-across box with $B_{upstream}/B_{target}=2$.

This has been further confirmed by predictive, full-geometry SOLPS-ITER modelling of the MAST-U divertor [5],[6]. As shown in figure 1b, a factor 2.4 higher $n_{upstream}$ was required for target electron flux rollover in the conventional divertor configuration (shown in red in figure 1a), compared to the Super-X configuration (shown in blue). From the difference in total flux expansion between these two configurations alone, equation (1) would predict a factor 1.88 increase in required $n_{upstream}$, and further analysis showed that total flux expansion was indeed the primary driver of the reduced $n_{upstream}$ at rollover in the Super-X.
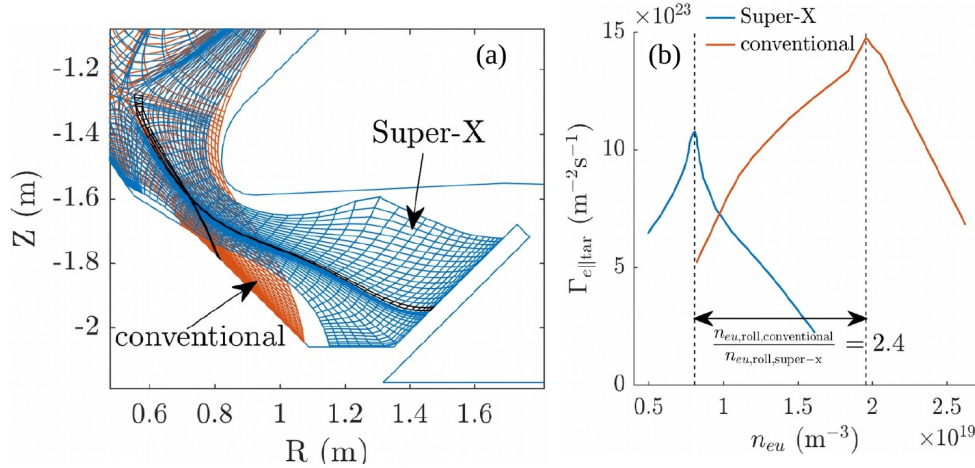

FIG 1: MAST-U predictive modelling of target electron flux rollover in Super-X and conventional geometries, as a function of upstream electron density. Values in (b) are plotted for the 3rd flux tubes in both configurations, highlighted in black in (a). Reproduced with permission from [6].

Despite these apparently strong pieces of theoretical evidence that total flux expansion should allow for lower upstream detachment onset densities, the experimental evidence on TCV suggests, if anything, the opposite trend. It was shown in experiments without divertor baffling [7], that the outer target actually rolls over at a slightly *higher* upstream density when R_{target} is increased.

In order to understand this experimental result, interpretative simulations of the same R_{target} scan on TCV were carried out using SOLPS-ITER [8]. As shown in figure 2a, these successfully reproduced the unexpected experimental trend, whereby the low R_{target} case actually required a 30% *lower* upstream density to rollover, compared to a 30% *higher* upstream density predicted by (1). In this figure, the target ion flux density (on the flux tubes where the peak heat flux is located during the attached phase) is shown as a function of the outer mid-plane separatrix density, for the low-R_{target} and high-R_{target} configurations. The numerical grid used for each rollover plot is shown directly above and linked with an appropriately-coloured arrow.

D. MOULTON et al.

[Left hand page running head is author's name in Times New Roman 8 point bold capitals, centred. For more than two authors, write
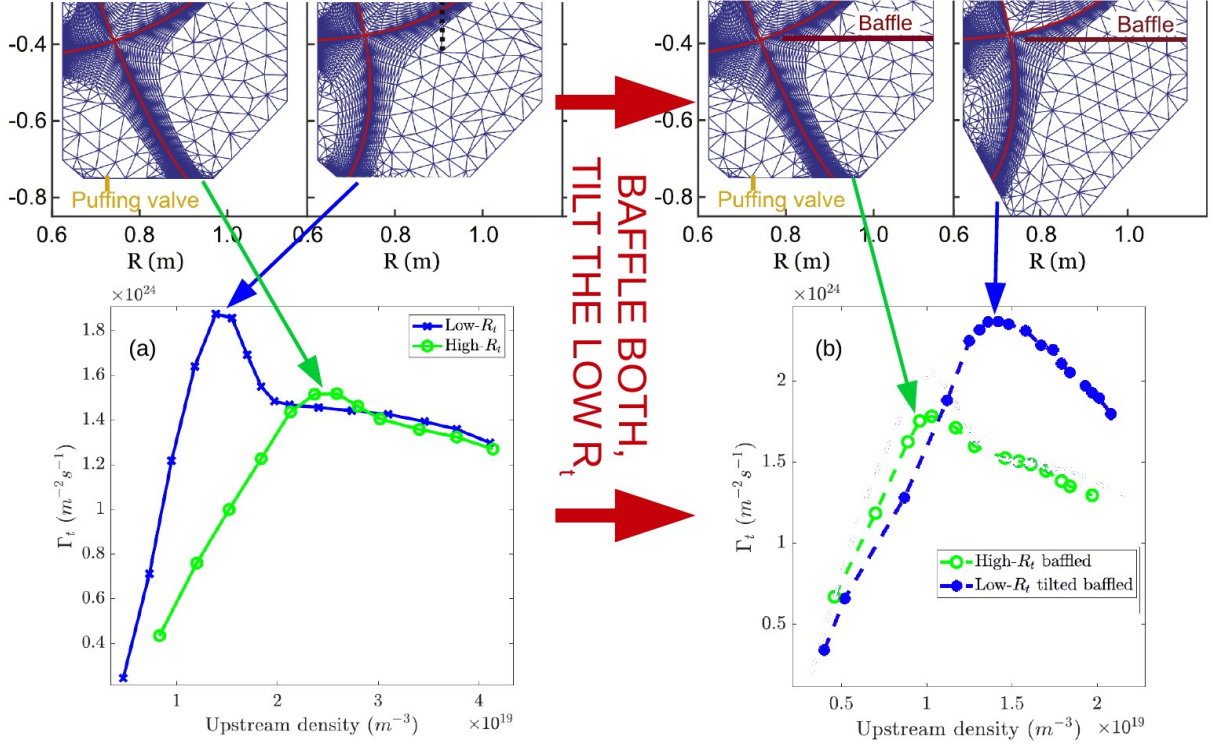**AUTHOR et al.**]

FIG 2: The geometries employed in the interpretative TCV SOLPS-ITER simulations, above the simulated ion target flux rollover in each geometry. Baffling both divertors and tilting the low R_{target} simulation was seen to reverse the trend in upstream rollover density. "Upstream density" here refers to the outer mid-plane separatrix density. Presentation modified, with permission, from figures shown in [8].

Having obtained this match to the experiment, a code experiment was carried out in an attempt to equalise the neutral trapping between the two configurations. To do this, a baffling surface was inserted into both divertor simulation grids, and the target of the low R_{target} case was tilted so that its poloidal inclination angle was the same as that for the high R_{target} case (figure 2b, top). In so doing, we were able to recover the expected trend according to equation (1) (figure 2b, bottom). Now, the low R_{target} case required a 50% higher upstream density to rollover, compared to a 30% higher upstream density predicted by (1). It remains to be seen whether the effect of total flux expansion alone can be sufficiently well isolated in experiment as in the simulations.

The main conclusion of the work described in [8] is that, on TCV, differences in neutral trapping between configurations can outweigh differences in total flux expansion in setting the upstream density required for ion target flux rollover. A combination of high neutral trapping (brought about through baffling and/or target tilting) and high total flux expansion is likely to be optimal in terms of achieving detachment onset. This is the situation on MAST-U (which, as a spherical tokamak, can more easily achieve large $R_{target}/R_{upstream}$ compared to a large aspect ratio machine, without requiring expensive enlargements of the toroidal field coils). It should be pointed out, however, that it is not clear whether the benefits of neutral trapping observed on current machines will scale to reactors.

3. DETACHMENT LOCATION SENSITIVITY

Controlling the location of the detachment front in a reactor will be important[†]. Too close to the target and there is a risk of radiative, neutral and surface recombination target loads remaining too high, as well as a greater susceptibility to transients. Too far from the target and there is a risk of significant radiation from closed field lines, possibly dropping the separatrix power below the H-to-L "back transition" power threshold, P_{H-L}, and/or worsening helium divertor compression and pumping. For a reactor whose P_{H-L} is close to its heating power, the ideal situation would be to hold the detachment front at some predetermined location up the divertor leg, where the trade off between these goals is optimised.

Detachment front location sensitivity and detachment front control are closely linked; a detachment front that is insensitive to plasma control parameters can be easily controlled, and vice versa. In work that is soon to be submitted [9], we took the Super-X fuelling scan performed in [6] and carried out a nitrogen seeding scan from an attached unseeded simulation. Figure 3a shows the locations of the T_e=5 eV fronts as the nitrogen seeding rate was increased with equally-sized steps. Note that the evolution of the fuelling scan detachment fronts are also discussed in [9]. They followed a similar pattern but for brevity we focus on the seeding scan here.

Figure 3b shows the evolution of variously-defined detachment fronts as a function of a normalised "lumped control parameter". This is given by

$$C_l = \frac{n_{\text{upstream}} \sqrt{f_{\text{eff}}}}{q_{\parallel,\text{upstream}}^{5/7}} \qquad (2)$$

and is based on the Detachment Location Sensitvity (DLS) model described in [3], which predicts the front location to be a function of C_l only[‡], for a given magnetic geometry. In [9], the model given in [3] has been generalised to include an arbitrary magnetic field profile along the flux tube of interest, allowing direct comparison between the simple model and the more complex SOLPS-ITER simulations. The generalised DLS model depends solely on the magnetic field profile and C_l. The DLS-predicted front location is plotted as a solid black line in figures 3b and 3c, as a function of parallel distance (l) and poloidal distance (l_{pol}) from the target, respectively. Note that here C_l has been normalised to its value when the 5 eV front is just on the verge of pulling away from the target.

FIG 3: (a) 2D T_e=5 eV front location as a function for stepwise increases in nitrogen seeding rate in the MAST-U Super-X divertor configuration. (b,c) The location of various definitions of the detachment front, as a function of the normalised lumped control parameter (see text for details). The simple DLS model prediction is also shown for comparison. Modified with permission from [9].

In figure 3b we see that, for all of the front definitions considered (Te=5 eV, maximum electron cooling due to deuterium atom ionisation $P_{H,\text{max}}$, 50% of $P_{H,\text{max}}$, or 50% of the maximum electron carbon radiation $P_{C,\text{max}}$), the position of the simulated detachment front becomes less sensitive to changes in C_l in regions of high magnetic field variation (i.e. high dB/dl, shaded grey in figures 3b and 3c). This is qualitatively consistent with the generalised DLS model, which also predicts a reduction in sensitivity in that region. Conceptually, this can be understood as a larger increase in radiation being required to drop $q_\parallel$ in regions where $q_\parallel$ is naturally rising quickly away from the target due to rapidly decreasing magnetic field strength. Note also that in general the simulations predict the front to be less sensitive to changes in control parameters (i.e. more easily controlled) than predicted by the generalised DLS model.
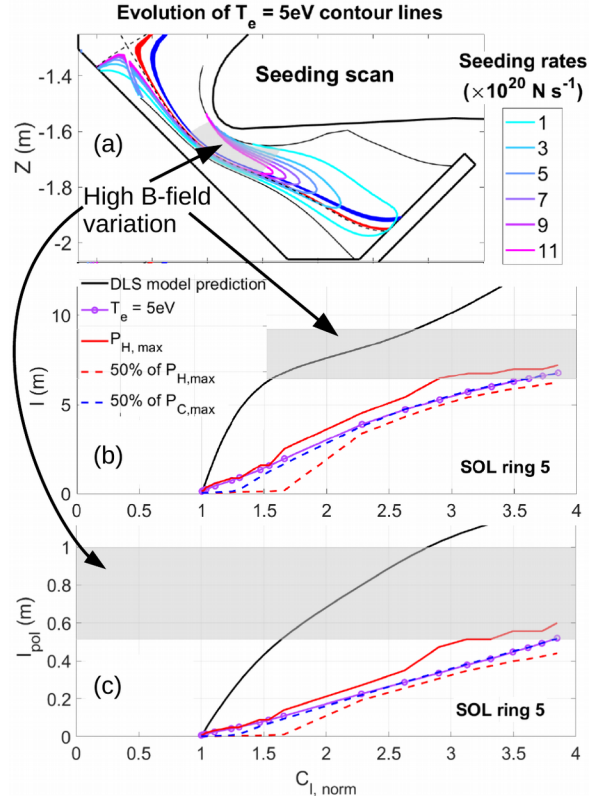

[†]The term "detachment front" tends to be used quite loosely in the field. We refer here to the T_e=5 eV front, unless otherwise stated.

[‡]f_{eff} here refers to an "effective radiating species fraction", which includes N, C and D radiation, and is defined such that, in the case where the C, N and D fractions are poloidally constant f_{eff} is just the sum of those fractions.

D. MOULTON et al.
[Left hand page running head is author's name in Times New Roman 8 point bold capitals, centred. For more than two authors, write
AUTHOR et al.]

When considering the slow down of the front in poloidal space, the predicted drop in sensitivity is much less pronounced, in both the generalised DLS model and the simulations (figure 3c). Ideally we would like to be able to control the detachment front in poloidal rather than parallel space; assuming toroidal symmetry, it is the poloidal distribution of the radiation in the leg that sets the loads on the divertor side walls as well as the neutral trapping in the divertor required for efficient helium pumping. Nevertheless, as seen in figure 3a, there is a clear drop in the sensitivity of the poloidal location of the front to nitrogen seeding rate once the front reaches the region of high B field variation. This is actually a result of the nitrogen concentration in the divertor becoming less sensitive to changes in the seeding rate, rather than the poloidal front location becoming less sensitive to the nitrogen concentration (it is not yet clear why this is the case).

As a final point of discussion on detachment location sensitivity, it should be noted that the X-point-radiating solution may actually turn out to be a good one on reactors with sufficiently low P_{H-L} (supposing the helium compression and pumping can be maintained), and has recently been observed in an ELM-suppressed regime on ASDEX Upgrade [10]. In that case, there is no need to spend money on an advanced divertor volume that is not dissipating power, at least in the absence of transients.

4. DEEP DETACHMENT

In addition to detachment onset and stability, it is also of interest to consider the deeply detached state itself, since this may well be a necessary state for reactors to operate in. This has been investigated in another soon-to-be-submitted study [11]. Figure 4, taken from that study, shows the particle balance for the entire outer divertor of the MAST-U fuelling scan ("puff scan", (a)) and nitrogen seeding scan ("seeding scan", (c)). These were the same scans analysed in the location sensitivity study summarised in the previous section. To gain further insight, an additional puff scan was carried out in the absence of deuterium ion-molecule elastic collisions. The deeply detached simulations chosen for further analysis are shown as stars. These all had very similar detachment front locations at ~7 m parallel distance from the target, as measured either by the Te=5 eV location, or by the location where convective heat flux takes over from conductive (these two definitions were found to be equivalent).
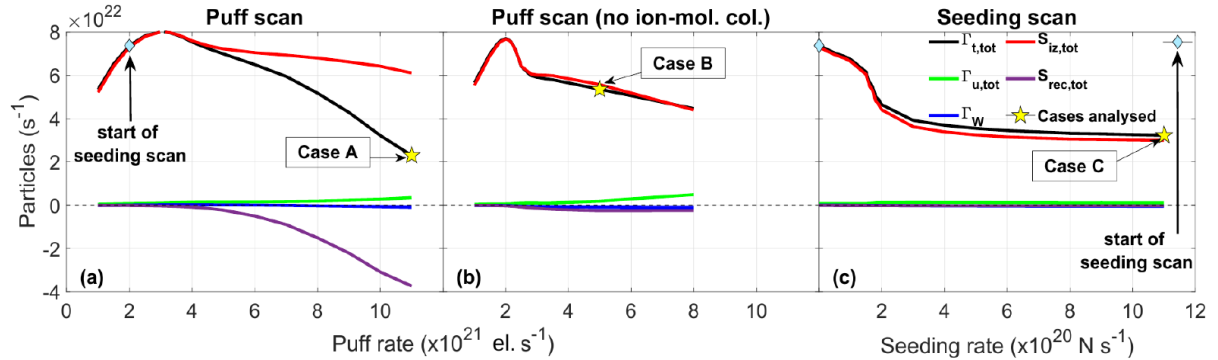

FIG 4: Particle balance in the entire MAST-U outer divertor, for (a) the reference D2 puff scans, (b) the D2 puff scan without deuterium ion-molecule elastic collisions, and (c) the nitrogen seeding scan. Here, Γ_w and $\Gamma_{u,tot}$ are the fluxes through the radial sides of the grid and the upstream flux into the divertor, respectively. Other quantities defined in the text. Reproduced with permission from [11].

There is an important difference between the deeply detached simulation driven by D_2 fuelling (case A) and the deeply detached simulation driven by N seeding (case C). The fuelling-driven case has a significant recombination sink ($S_{rec,tot}$ in figure 4), which amplifies the rollover in target particle flux (Γ_{ttot} in figure 4). In contrast, recombination in the seeding-driven case is negligible; the reduction in Γ_{ttot} aligns closely with the reduction in ionisation source ($S_{iz,tot}$ in figure 4). This diminished role of recombination for seeding compared to fuelling scans is qualitatively in line with experimental trends observed on C-mod [12] and TCV [13].

Deuterium ion-molecule elastic collisions play an important role in this qualitative difference between the two scans. This is clearly demonstrated by the equivalent puff scan in which those collisions were turned off (figure 4b). In that case, we observed no significant recombination in the deeply detached simulation (case B), even though the front location was at the same position and the upstream density was at the same value as in case A.

Figure 5 shows the profiles of (a) the recombination sink and (b) n_e and T_e, for these deeply detached simulations, along the 5ᵗʰ SOL flux ring (for which the target particle flux was maximum before detachment). The increased recombination sink, peaked right by the target, is clearly visible in the fuelling-driven case A. A

clear drop in T_e within 1 m of the target is also seen in the fuelling-driven case A, but not in the seeding-driven case C, nor the fuelling-driven case without ion-molecule collisions (case B). Power balance analysis to be presented in [11] shows that the dominant heat loss mechanism in that near-target region is from the ion channel due to ion-molecule elastic collisions. In addition, momentum loss due to the same ion-molecule elastic collisions slows the plasma towards the target in the fuelling-driven case, so that (to meet particle balance in particle-source-free region between the ionising and recombining zones) the electron density increases towards the recombining region. This combination of low T_e and high n_e, due apparently to heat and momentum removal by ion-molecule elastic collisions, respectively, allows recombination to become significant in the fuelling-driven case. Further work is required to test this trend experimentally, and to determine its reactor relevance.
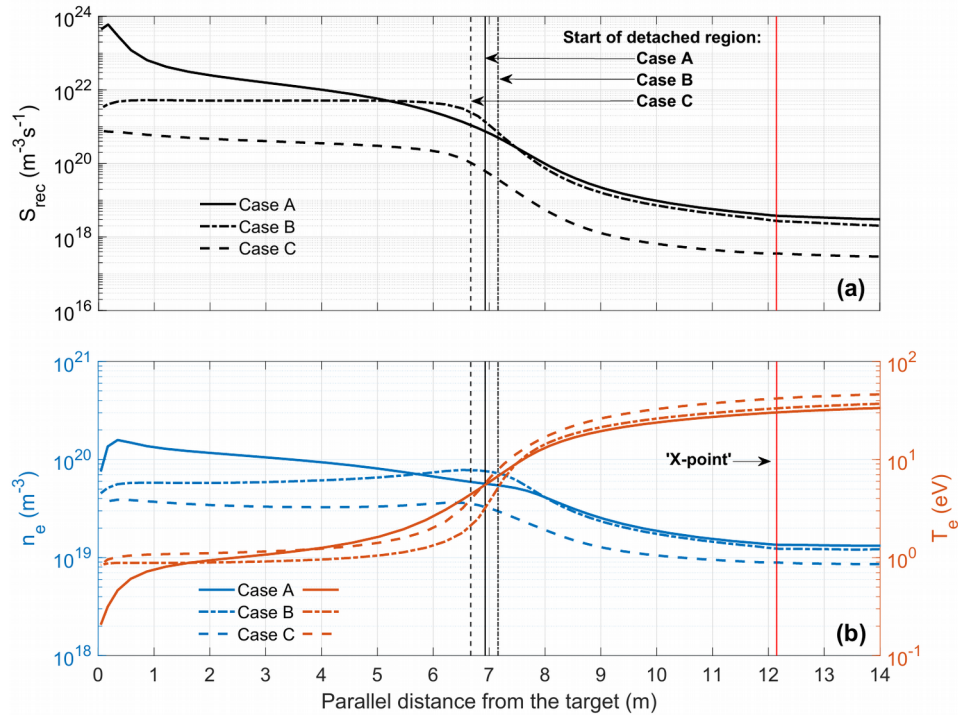

FIG 5: Parallel profiles of (a) the recombination sinks and (b) the electron densities and temperatures, for the deeply detached simulations marked with stars in figure 4. The start of the detached region, defined as the location where the convective heat flux becomes equal to the conductive heat flux, is marked by parallel black lines and is similarly-located in all three cases. Reproduced with permission from [11].

D. MOULTON et al.
[Left hand page running head is author's name in Times New Roman 8 point bold capitals, centred. For more than two authors, write
AUTHOR et al.]

5. REACTOR RELEVANCE

The work reviewed above suggests important potential benefits for long-legged divertors in current machines, but it is important to understand how this translates to fusion reactors. As part of the EUROfusion work package WP-DTT1/ADC [14], an engineeringly-plausible long-legged "Super-X" (SX) divertor for DEMO was compared to the conventional single null (SN) divertor [15]. The SN is essentially a scaled-up version of the ITER divertor in terms of its geometry, while the SX has its outer leg brought out to a higher major radius, leading to a ~30% increase in total flux expansion and a ~75% increase in outer connection length (note that, due to its large major radius, on DEMO it is considerably more cost effective to increase parallel connection length, rather than total flux expansion). Figure 6a compares the two geometries.
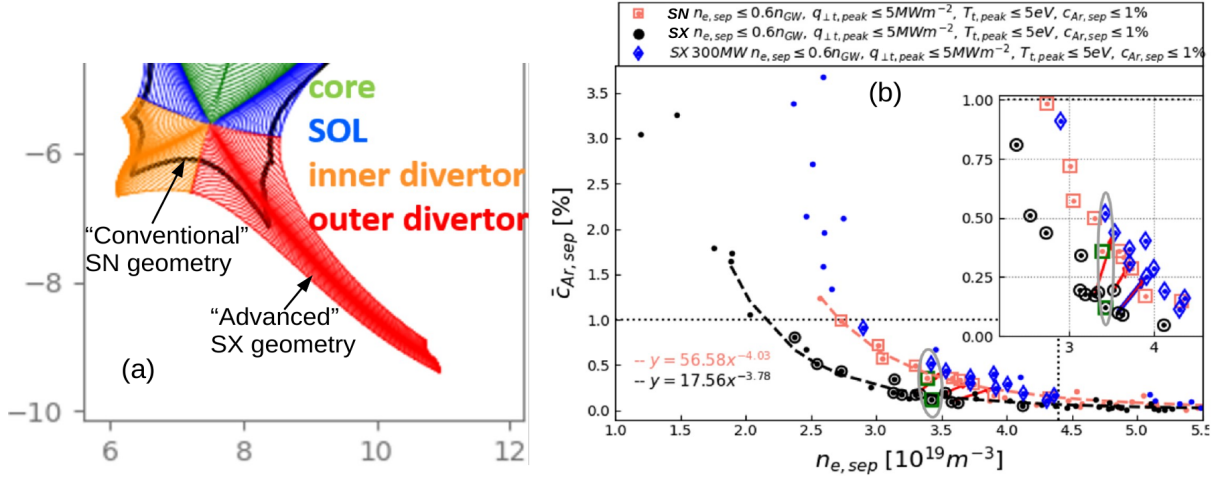

FIG 6: (a) The ITER-like SN divertor geometry (black) and the SX divertor (coloured). (b) All simulations in the performed matrix scan in deuterium puff and argon seeding. The average argon concentration on the portion of the separatrix vertically above the X-point, is plotted as a function of the electron density at the outer mid-plane separatrix. Each dot is a converged simulation. Dots with surrounding squares, circles or diamonds fall inside the operational space. Inset is a zoomed-in version of the same data, focussing on the operationally-viable simulations. Dashed lines are fitted to the data in the operational space with the expressions given in the bottom left. Other annotations relate to the specific simulations that were analysed in more detail in [15]. Reproduced with permission from [15].

SOLPS-ITER "matrix scans" in deuterium fuelling and argon seeding were carried out in both geometries, with an input power into both grids of 150 MW, with fluid neutrals, bundled argon charge states, λ_q=3 mm and in the absence of drifts. In SX, an additional matrix scan at 300 MW was also carried out. In figure 6b, the resulting argon concentrations on the separatrix $\bar{c}_{Ar,sep}$ (averaged over the portion vertically above the X-point) are plotted as a function of the separatrix electron density at the outer mid-plane $n_{e,sep,OMP}$, for the three matrix scans. Points surrounded by squares, circles, or diamonds, have tolerable exhaust conditions (peak target heat load on either target ≤ 5 Mwm^{-2} and peak target ion temperature ≤ 5 eV). They also have tolerable core boundary conditions (somewhat arbitrary cut offs of $n_{e,sep,OMP} < n_{GW}$, where n_{GW} is the Greenwald density, and $\bar{c}_{Ar,sep} \leq 1\%$).

The key conclusions from figure 6b are: (i) for the same $n_{e,sep,OMP}$ ($\bar{c}_{Ar,sep}$), the SX (black circles) required a factor ~0.5 lower $\bar{c}_{Ar,sep}$ (~0.8 lower $n_{e,sep,OMP}$) to achieve operationally-tolerable exhaust conditions, compared to the SN (pink squares); (ii) The SX with 300 MW input power required only slightly higher $n_{e,sep,OMP}$ and $\bar{c}_{Ar,sep}$ compared to the SN with 150 MW input power. Both of these conclusions can be broadly explained by simple 'Lengyel Model' considerations which, in the absence of total flux expansion and for constant impurity enrichment, predicts

$$q_{\parallel u}^{4/3} \bar{c}_{Ar,sep}^{-7/6} n_{e,sep,OMP}^{-7/3} \propto L_{\parallel} \tag{3}$$

for the conditions required to exhaust all of the input power through radiation (equation (3) was derived by taking equation (8) of [16] with $L_{INT} \propto T_u$ assumed for argon and $T_u \propto (q_{\parallel u} L_{\parallel})^{2/7}$). That is, a factor 1.75 increase in $L_{\parallel}$ for the SX would be predicted to allow a factor 1.52 higher $q_{\parallel u}$, or a factor 0.62 lower $\bar{c}_{Ar,sep}$, or a factor 0.79 lower $n_{e,sep,OMP}$. The improved performance of the SX can be largely attributed to it's increased connection length rather than its mildly increased total flux expansion. Further work is required to understand if these improvements are actually necessary for DEMO to achieve its goals. Note that initial analysis suggests that simple arguments relating inner/outer connection length ratios to inner/outer power asymmetries (which would predict higher inner target loading in SX compared to SN) do not hold in these simulations, due to the presence of near-SOL parallel currents which drive a significant convective electron energy flux towards the outer divertor in SX but not in SN.

6. SUMMARY

This paper has summarised recent work, performed by UKAEA and the University of York, to simulate long legged divertors and investigate their potential benefits for reactors. Simulations and simple models predict total flux expansion eases access to detachment, and interpretative modelling is able to explain why so far this has not been experimentally observed on TCV, due to neutral trapping effects. Early indications on MAST-U are that total flux expansion is indeed important, and our future efforts will focus on interpreting those experiments through SOLPS modelling.

Detachment front sensitivity is another key area where long-legged divertors could potentially provide benefit over conventional divertors. In line with simple models, our predictive SOLPS-ITER simulations of the MAST-U Super-X divertor suggest a slowing down in parallel space of the detachment front in regions of high magnetic field strength gradient. Future work will aim towards verifying this experimentally on MAST-U and exploring magetic geometries which reduce sensitivity to the "lumped control parameter" (equation (2)) in poloidal space rather than (or as well as) in parallel space.

Our analysis of deeply detached MAST-U Super-X simulations suggests that, at the input powers initially available on MAST-U, there will be a clear qualitative difference between deeply detached states achieved via nitrogen seeding (i.e. lower upstream density, higher impurity concentration) and equally deeply detached states achieved via deuterium fuelling (i.e. higher upstream density, lower impurity concentration). We predict that strong recombination sinks will be observed in MAST-U for the fuelling-driven detachment cases but not for detachment driven by nitrogen seeding, and simulations suggest that the poloidal density profiles will be peaked near the target but flat in the seeding-driven case. In the simulations, deuterium ion-molecule collisions are necessary for this difference to arise.

Regarding the relevance of long-legged divertors to reactors, efforts have been made within the Eurofusion work package WP-DTT1/ADC to simulate an engineeringly-feasible long-legged divertor on DEMO. This work suggests a significant improvement in operational margin, compared the the standard ITER-like DEMO divertor, due primarily to the presence of a longer connection length (only a 30% increase in total flux expansion was deemed feasible due to limited space inside the toroidal field coils). The improvements are in line with those expected from simple Lengyel Model calculations. Further work is required to understand if this improved margin is necessary for DEMO to meet its design criteria.

REFERENCES

[1] KOTSCHENREUTHER, M et al. (2010) Nucl. Fusion **50** 035003

[2] PETRIE, T W et al. (2013) Nucl. Fusion **53** 113024

[3] LIPSCHULTZ, B et al. (2016) Nucl. Fusion **56** 056007

[4] MOULTON, D et al. (2017) PPCF **59** 065011

[5] HAVLICKOVA, E et al. (2015) PPCF **57** 115001

[6] MOULTON, D et al. (2017) "Detachment onset in MAST-U according to SOLPS-ITER". Proc. 44th EPS Conference on Plasma Physics

[7] THEILER, C et al. (2017) Nucl. Fusion **57** 072008

[8] FIL, A et al. (2020) PPCF **62** 035008

[9] MYATRA, O et al. (2021) to be submitted

[10] BERNERT, M et al. (2021) Nucl. Fusion **61** 024001

[11] MYATRA, O et al. (2021) to be submitted

[12] LIPSCHULTZ, B et al. (1999) Phys. Plasmas **6** 1907

[13] VERHAEGH, K et al. (2019) Nucl. Fusion **59** 126038

[14] MILITELLO, F et al. (2021) Nucl. Mater. En. **26** 100908

[15] XIANG, L et al. (2021) submitted to Nucl. Fusion

[16] REINKE, M et al (2017) Nucl. Fusion **57** 034004